Supplementary Information

Novel Amino Acid Derivatives of Quinolines as Potential Antibacterial and Fluorophore Agents

Oussama Moussaoui[1,*], Rajendra Bhadane[2,3], Riham Sghyar[1], El Mestafa El Hadrami[1], Soukaina El Amrani[4], Abdeslem Ben Tama[1], Youssef Kandri Rodi[1], Said Chakroune[1], Outi M. H. Salo-Ahen[2,3,*]

[1] Laboratory of Applied Organic Chemistry, Sidi Mohamed Ben Abdellah University, Faculty of Sciences and Techniques, 30000 Fez, Morocco
[2] Structural Bioinformatics Laboratory, Faculty of Science and Engineering, Biochemistry, Åbo Akademi University, FI-20520 Turku, Finland
[3] Pharmaceutical Sciences Laboratory, Faculty of Science and Engineering, Pharmacy, Åbo Akademi University, FI-20520 Turku, Finland
[4] Laboratory of Materials, Processes, Catalysis and Environment. Bioindustry and Agri-Food Technology team, Higher School of Technology, Sidi Mohamed Ben Abdellah University, 30000 Fez, Morocco

*Correspondence: oussama.moussaoui1208@gmail.com; outi.salo-ahen@abo.fi; Tel.: +212654496534 (O.M.); +358-2-2154009 (O.M.H.S.-A.)

Table of Contents

Figures

Identification of putative ligand binding sites at DNA gyrase (Figures S1 and S2)

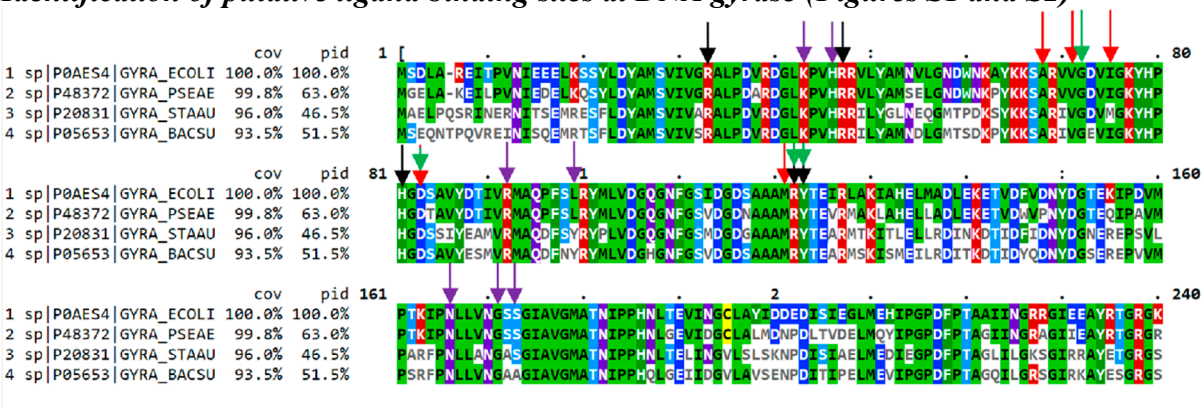

Figure S1. Multiple sequence alignment of DNA gyrase subunit A (GyrA) of *E. Coli, P. aeruginosa, S. aureus, B. subtilis* (1 to 4, respectively). The arrows indicate the interaction sites with co-crystallised ligands in the selected crystal structures of the proteins (purple and black arrows: antibiotic simocyclinone D8 binding site formed by both GyrA chains, A and B, respectively (PDB ID: 2Y3P[1]); red arrows: binding site of novel bacterial topoisomerase inhibitors (NBTIs) (PDB IDs: 5BS3[2] and 4PLB[3]); green arrows: gepotidacin binding site (PDB ID: 6QTP[4]).

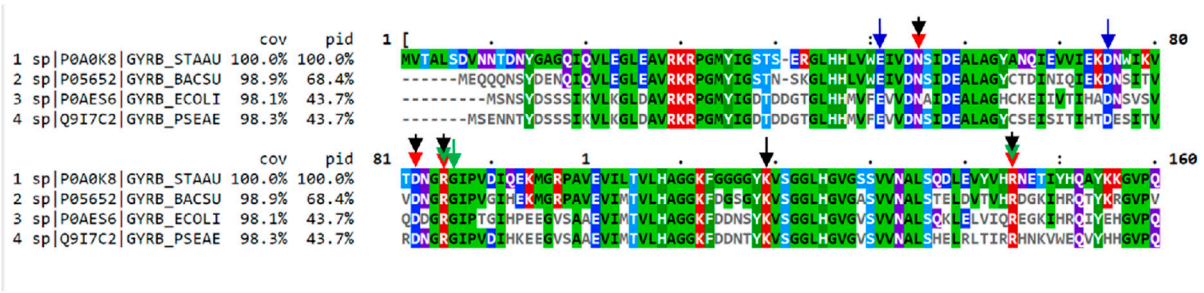

Figure S2. Multiple sequence alignment of DNA Gyrase subunit B (GyrB) of *S. aureus*, *B. subtilis*, *E. Coli*, *P. aeruginosa* (1 to 4, respectively). The arrows indicate the interaction sites with co-crystallised ligands in the selected crystal structures of the proteins; blue arrows: ATP-binding site (PDB ID: 4PRX[5]); green arrows: novobiocin binding site (PDB ID: 1AJ6[6]); black arrows: coumermycin A1 binding site (PDB ID: 6ENG[7]); red arrows: indolinone fragment 1 binding site (PDB ID: 5CPH[8]) and pyrrolamide inhibitor 26 binding site (PDB ID: 3TTZ[9]).

Ligand-receptor interaction diagrams over MD simulations (Figures S3-S6)

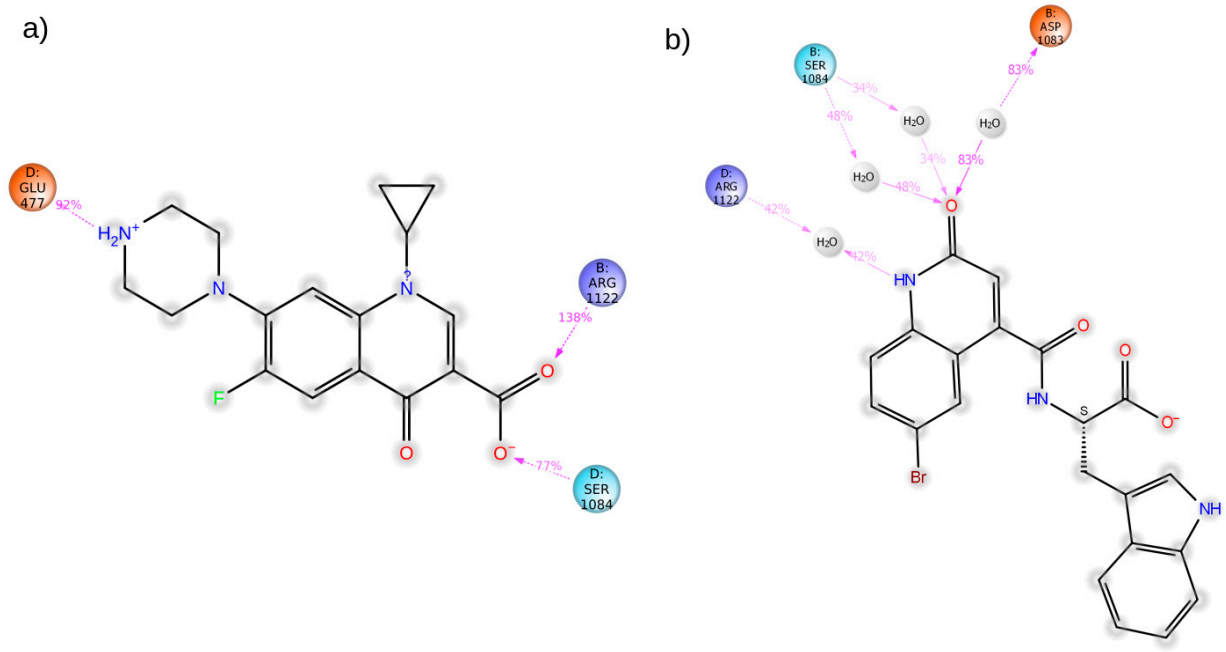

Figure S3. Ligand-receptor interaction diagrams at the fluroquinolone binding site of *S. aureus* DNA-gyrase subunit A (PDB ID: 2XCT, B and D chains) over the course of a 10-ns molecular dynamics simulation (% denotes the duration of an interaction from the total simulation time). Only interactions that lasted for more than 30% of the simulation time are taken into account. (a) Co-crystallised ciprofloxacin; (b) compound 4e. DNA/ion interactions are not shown.

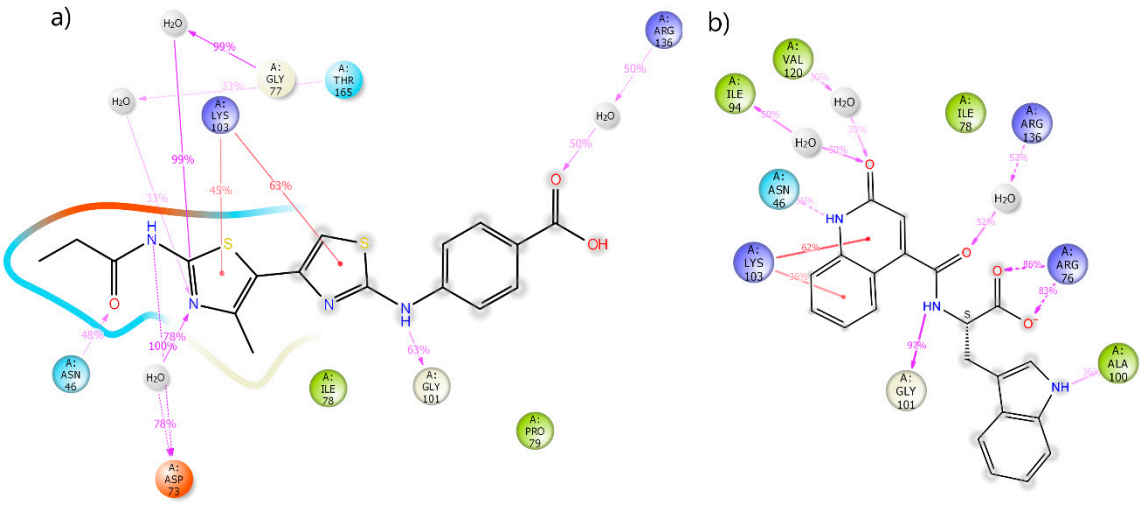

Figure S4. Ligand-receptor interaction diagrams at the coumarin binding site of *E. coli* DNA gyrase monomeric B subunit (PDB ID: 4DUH) over the course of a 10-ns molecular dynamics simulation (% denotes the duration of an interaction from the total simulation time). Only interactions that lasted for more than 30% of the simulation time are taken into account. (a) Co-crystallised 4,5'-bithiazole (inhibitor 18); (b) compound 3e.

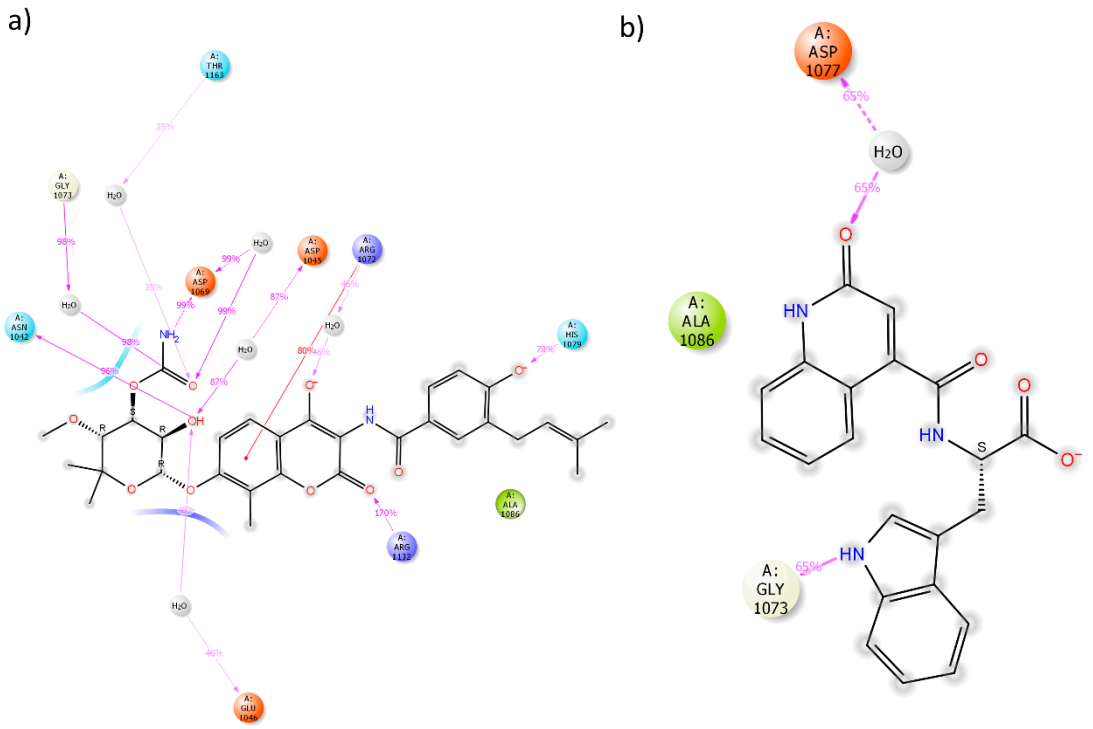

Figure S5. Ligand-receptor interaction diagrams at the coumarin binding site of *E. coli* DNA Topoisomerase IV ParE subunit (PDB ID: 1S14) over the course of a 10-ns molecular dynamics simulation (% denotes the duration of an interaction from the total simulation time). Only interactions that lasted for more than 30% of the simulation time are taken into account. (a) Co-crystallised novobiocin; (b) compound 3e.

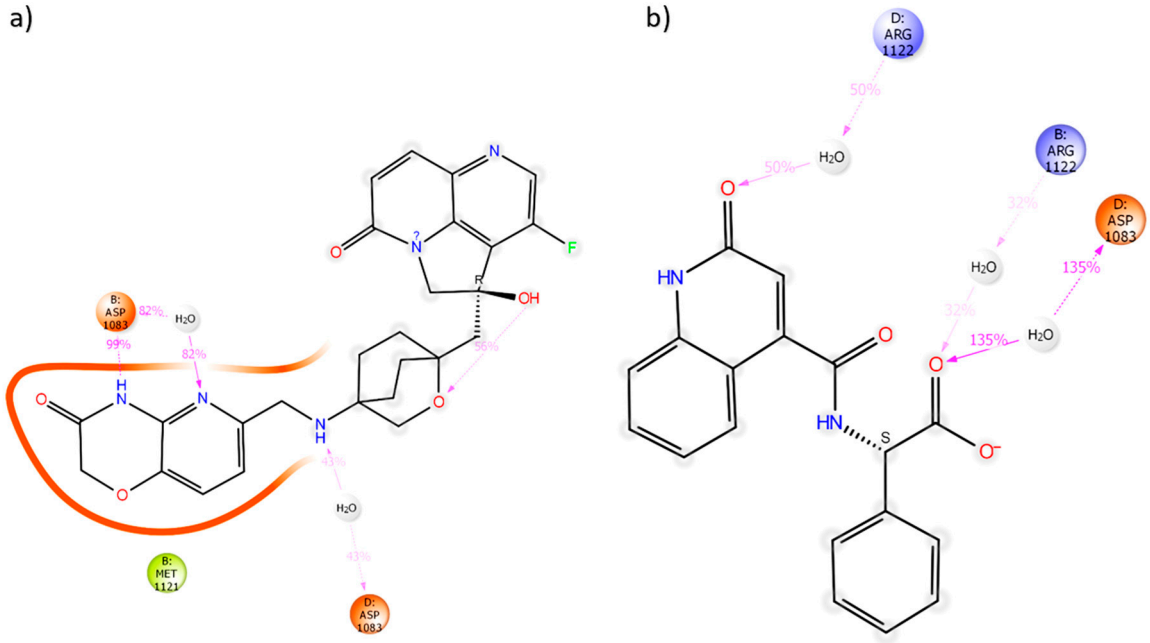

Figure S6. Ligand-receptor interaction diagrams at the NBTI site of the *S. aureus* DNA-gyrase subunit A (PDB ID: 5BS3, B and D chains) over the course of a 10-ns molecular dynamics simulation (% denotes the duration of an interaction from the total simulation time). Only interactions that lasted for more than 30% of the simulation time are taken into account. (a) Co-crystallised tricyclic-1,5-naphthyridinone (compound 7); (b) compound 3c.

Normalised ligand receptor interaction histograms over MD simulations (Figures S7-S10)

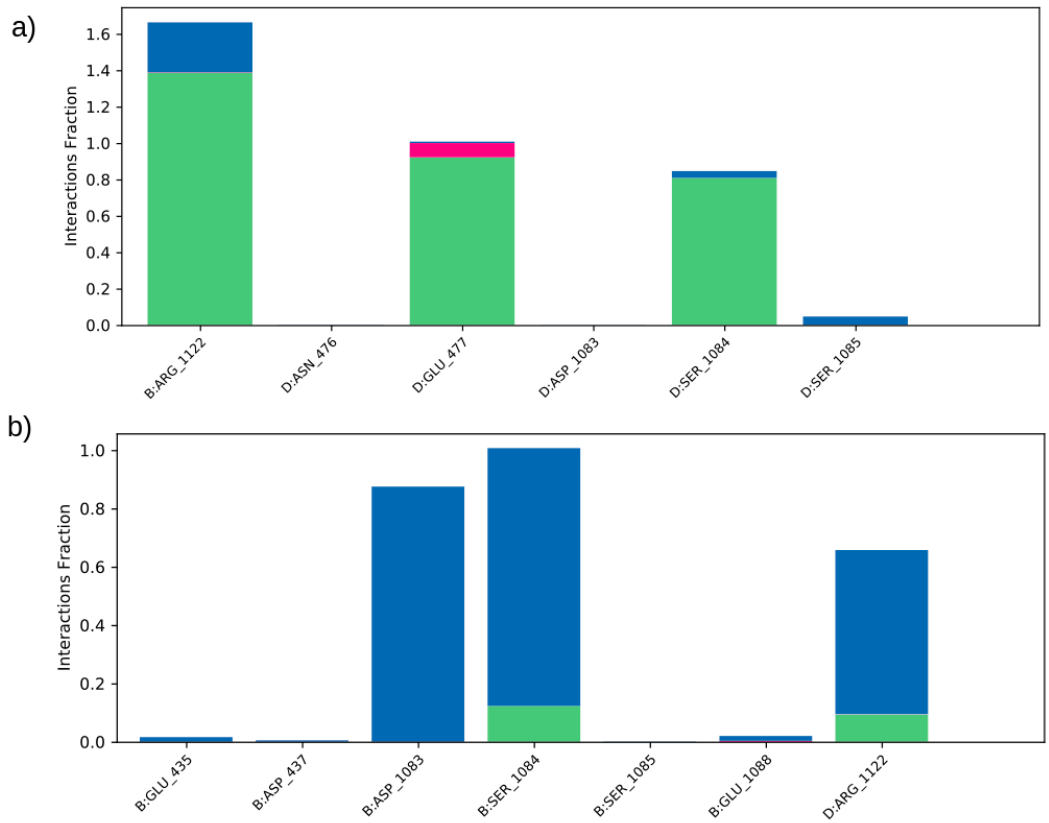

Figure S7. Ligand-receptor interaction histogram at the fluoroquinolone binding site of *S. aureus* DNA-gyrase subunit A (PDB ID: 2XCT, B and D chains). (a) Co-crystallised ciprofloxacin; (b) compound 4e. The stacked bar charts are normalized over the course of a 10-ns molecular dynamics simulation trajectory; thus, the interactions fraction value denotes how long the interaction lasted with respect to the length of the total simulation. Colour code: green – hydrogen bond interactions, blue – water-mediated interactions, purple – hydrophobic interactions, red – ionic interactions. Only interactions with amino acid residues are shown.

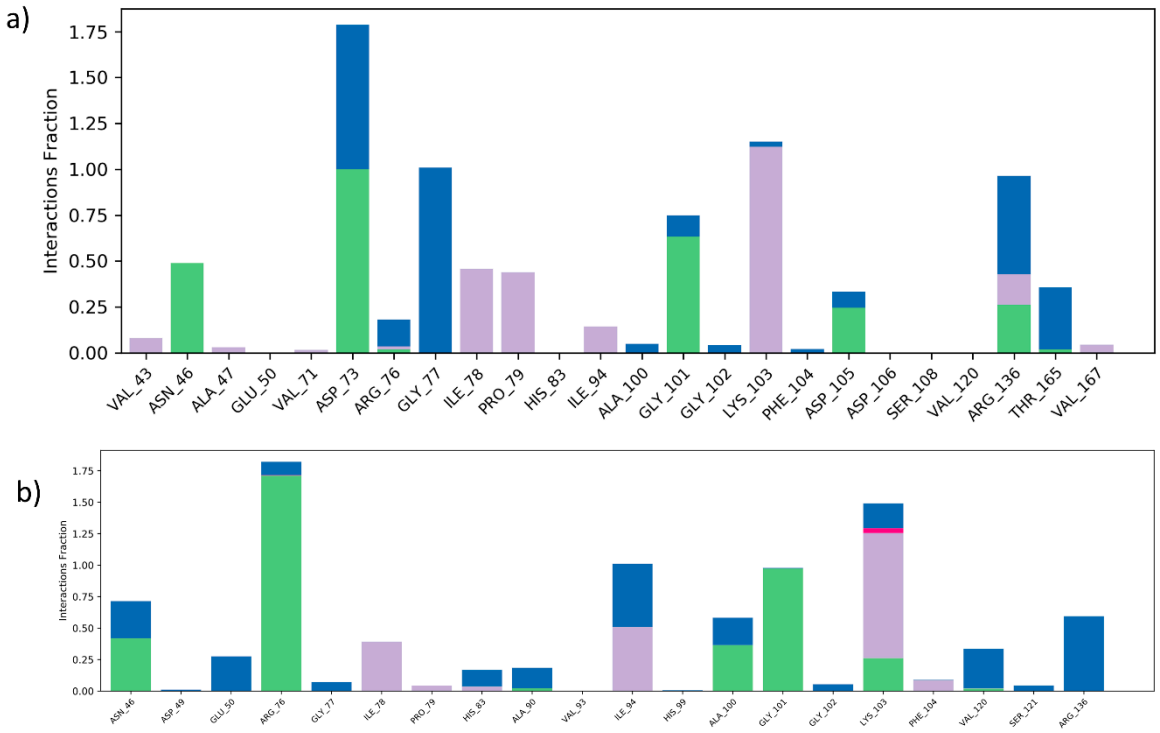

Figure S8. Ligand-receptor interaction histogram at the coumarin binding site of *E. coli* DNA gyrase monomeric B subunit (PDB ID: 4DUH). (a) Co-crystallised 4,5'-bithiazole (inhibitor 18); (b) compound 3e. The stacked bar charts are normalized over the course of a 10-ns molecular dynamics simulation trajectory; thus, the interactions fraction value denotes how long the interaction lasted with respect to the length of the total simulation. Colour code: green – hydrogen bond interactions, blue – water-mediated interactions, purple – hydrophobic interactions, red – ionic interactions. Only interactions with amino acid residues are shown.

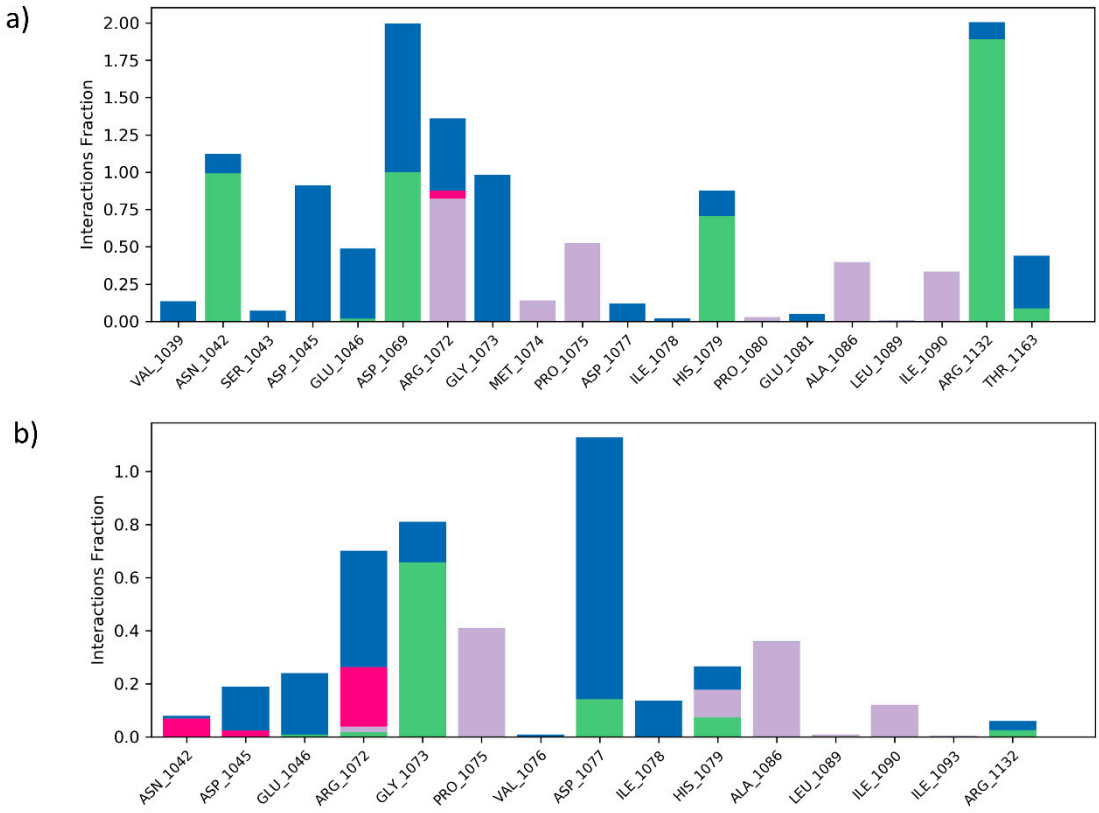

Figure S9. Ligand-receptor interaction histogram at the coumarin binding site of *E. coli* DNA Topoisomerase IV ParE subunit (PDB ID: 1S14). (a) Co-crystallised novobiocin; (b) compound 3e. The stacked bar charts are normalized over the course of a 10-ns molecular dynamics simulation trajectory; thus, the interactions fraction value denotes how long the interaction lasted with respect to the length of the total simulation. Colour code: green – hydrogen bond interactions, blue – water-mediated interactions, purple – hydrophobic interactions, red – ionic interactions. Only interactions with amino acid residues are shown.

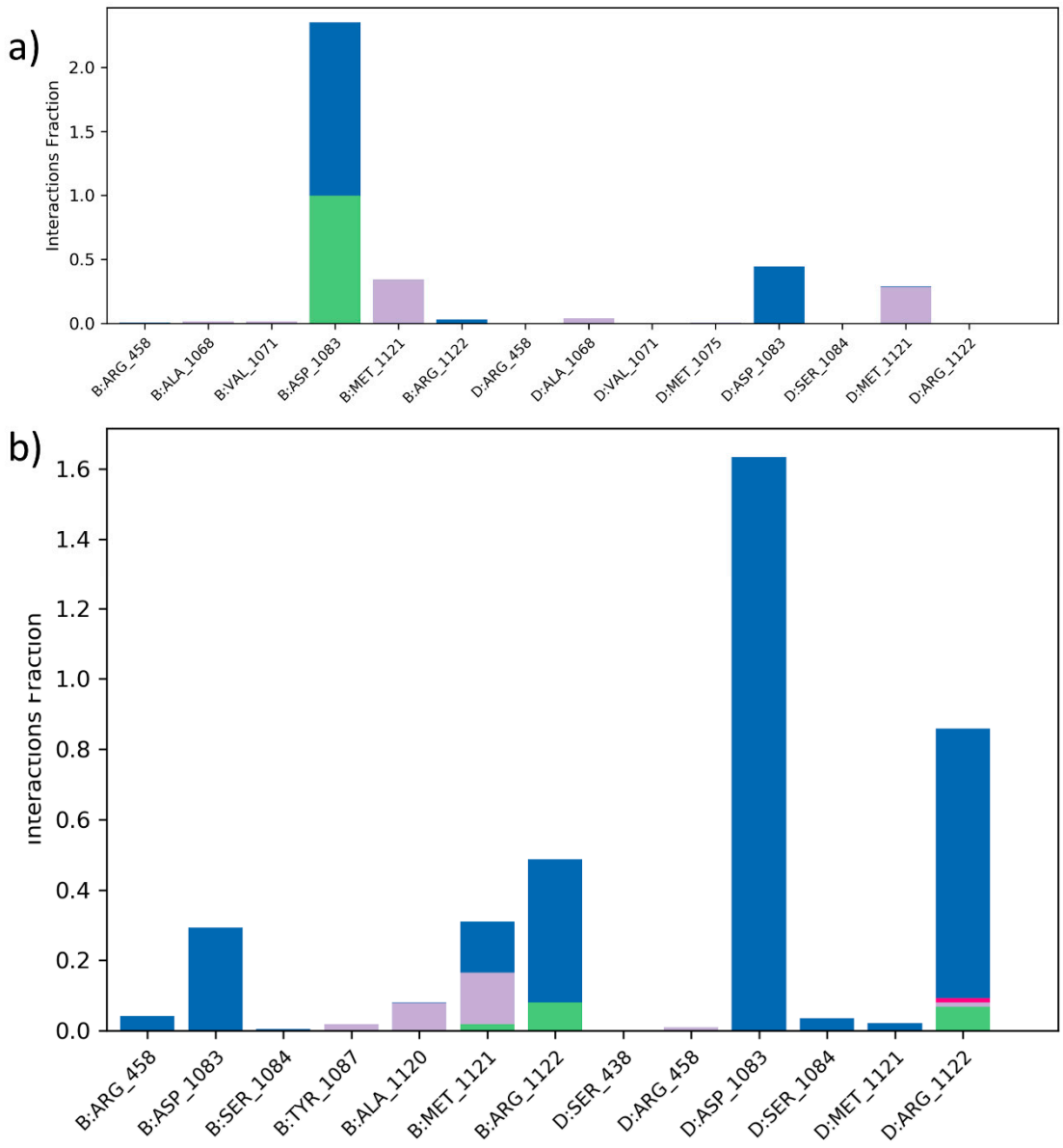

Figure S10. Ligand-receptor interaction histogram at the NBTI site of the *S. aureus* DNA-gyrase subunit A (PDB ID: 5BS3; B and D chains). (a) Co-crystallised tricyclic-1,5-naphthyridinone (compound 7); (b) compound 3c. The stacked bar charts are normalized over the course of a 10-ns molecular dynamics simulation trajectory; thus, the interactions fraction value denotes how long the interaction lasted with respect to the length of the total simulation. Colour code: green – hydrogen bond interactions, blue – water-mediated interactions, purple-hydrophobic interactions, red – ionic interactions. Only interactions with amino acid residues are shown.

RMSD plots of the ligand-receptor complexes over MD simulations (Figures S11-S14)

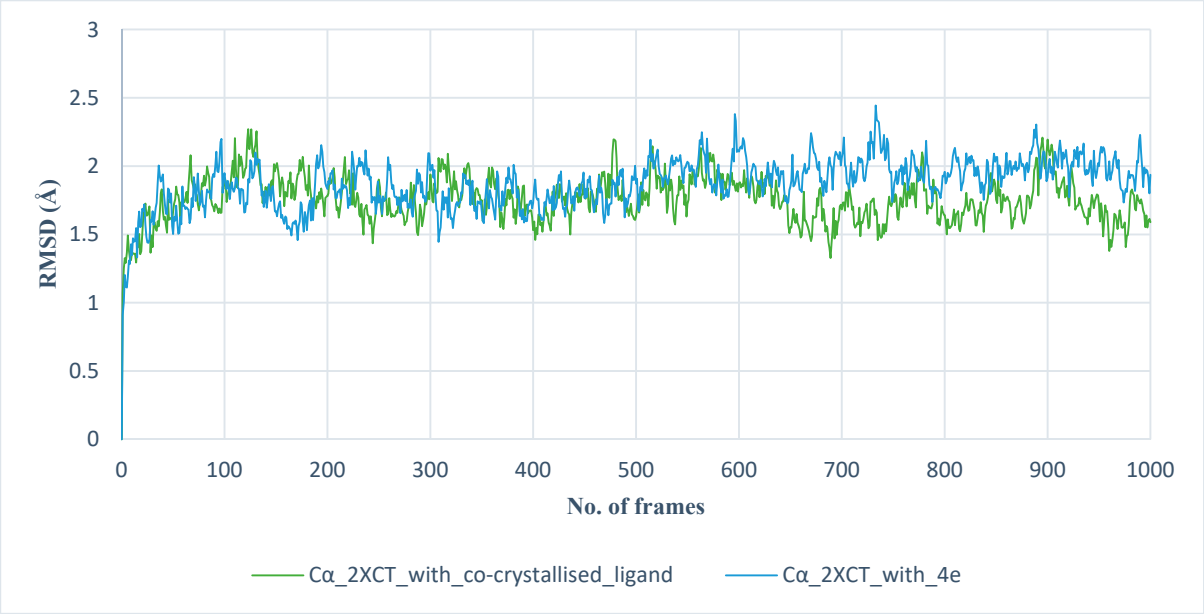

Figure S11. RMSD of the Cα atoms of *S. aureus* DNA gyrase subunit A (PDB ID: 2XCT) with a co-crystallised ciprofloxacin and compound 4e at the fluoroquinolone binding site.

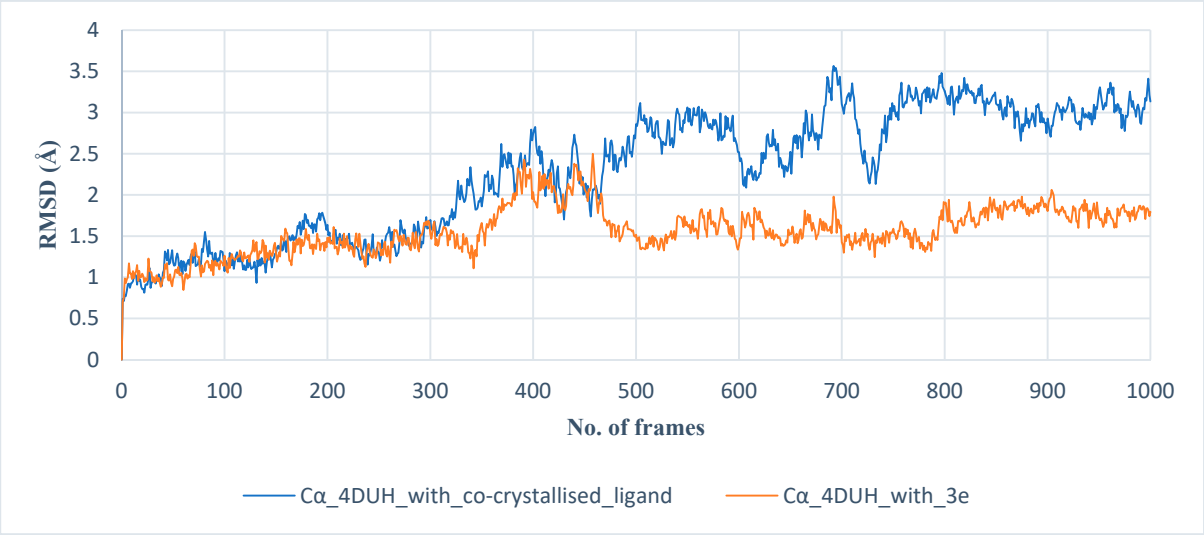

Figure S12. RMSD of the Cα atoms of *E. coli* DNA gyrase monomeric B subunit (PDB ID: 4DUH) with a co-crystallised 4,5'-bithiazole (inhibitor 18) and compound 3e at the coumarin binding site.

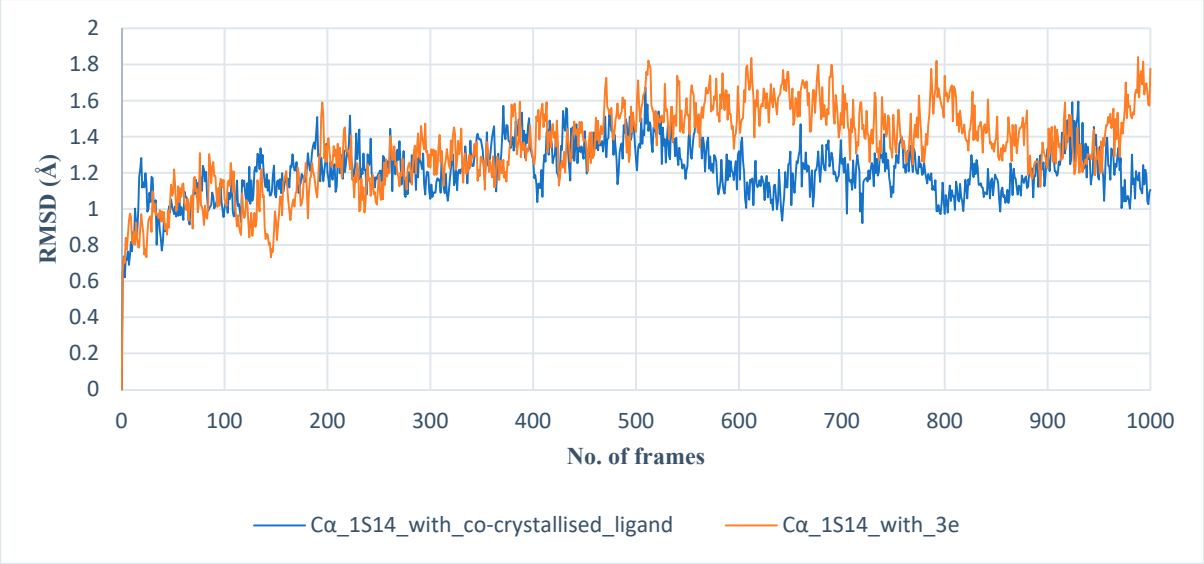

Figure S13. RMSD of the Cα atoms of *E. coli* topoisomerase IV ParE subunit (PDB ID:1S14) with co-crystallised novobiocin and compound 3e at the coumarin binding site.

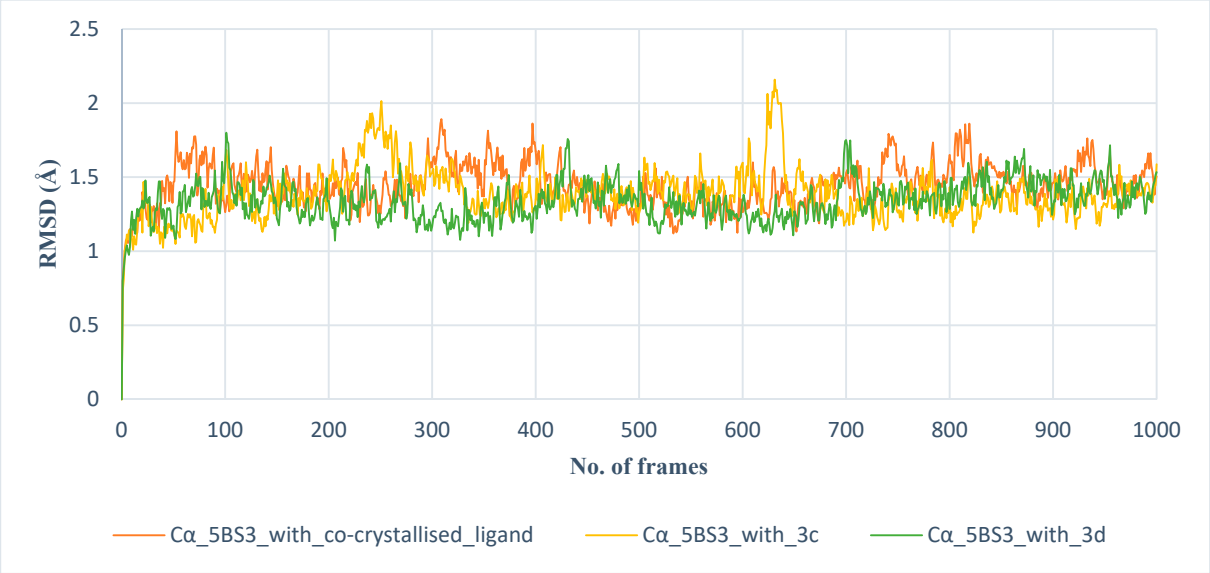

Figure S14 RMSD of the Cα atoms of *S. aureus* GyrA with co-crystallised tricyclic-1,5-naphthyridinone (compound 7) and compounds 3c and 3d at the NBTI site.

RMSF plots of the ligand-receptor complexes over MD simulations (Figures S15-S18)

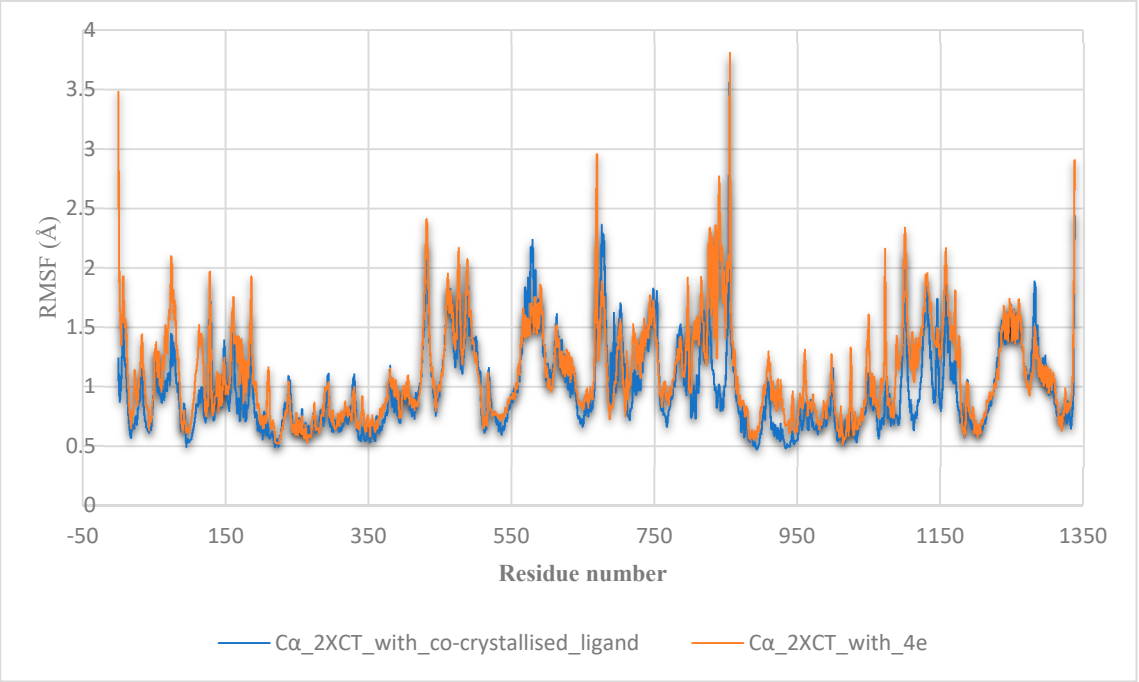

Figure S15. RMSF of the Cα atoms of *S. aureus* DNA gyrase subunit A (PDB ID: 2XCT) with the co-crystallised ciprofloxacin and compound 4e at the fluoroquinolone binding site.

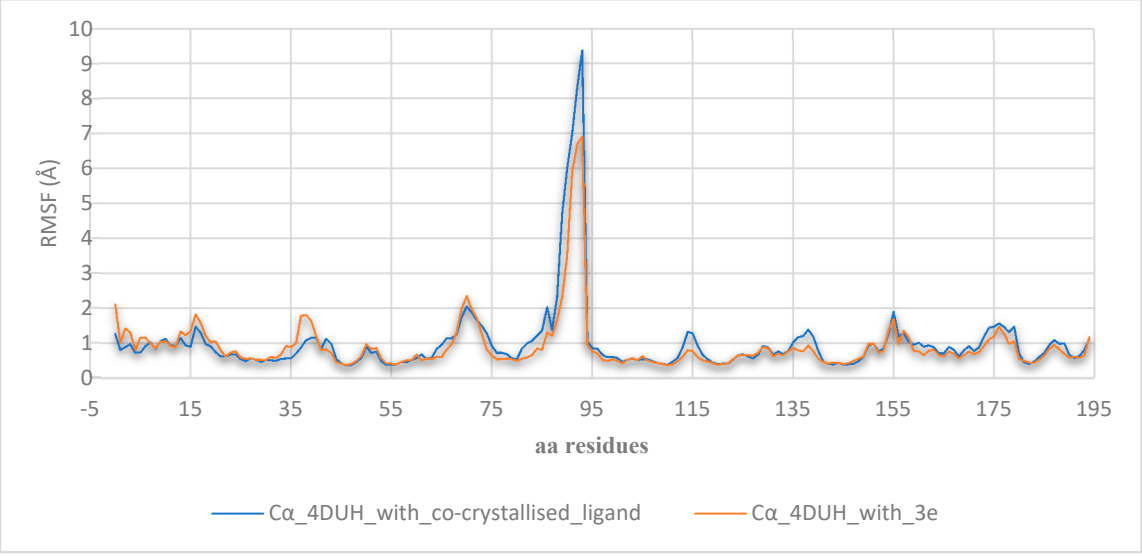

Figure S16. RMSF of the Cα atoms of *E. coli* DNA gyrase monomeric B subunit (PDB ID: 4DUH) with a co-crystallised 4,5'-bithiazole (inhibitor 18) and compound 3e at the coumarin binding site.

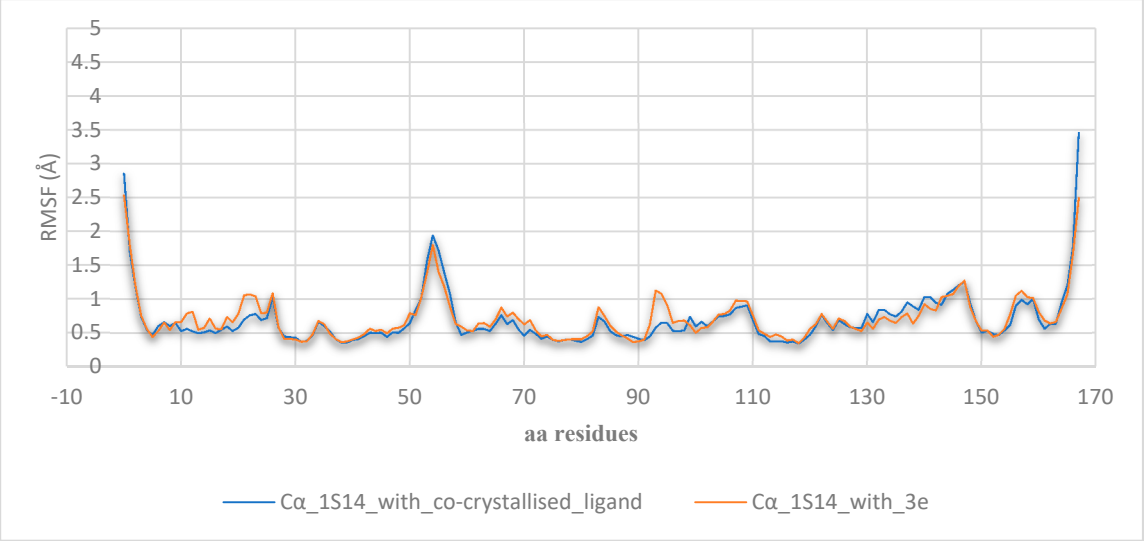

Figure S17. RMSF of the Cα atoms of topoisomerase IV ParE subunit (PDB ID:1S14) with co-crystallised novobiocin and compound 3e at the coumarin binding site.

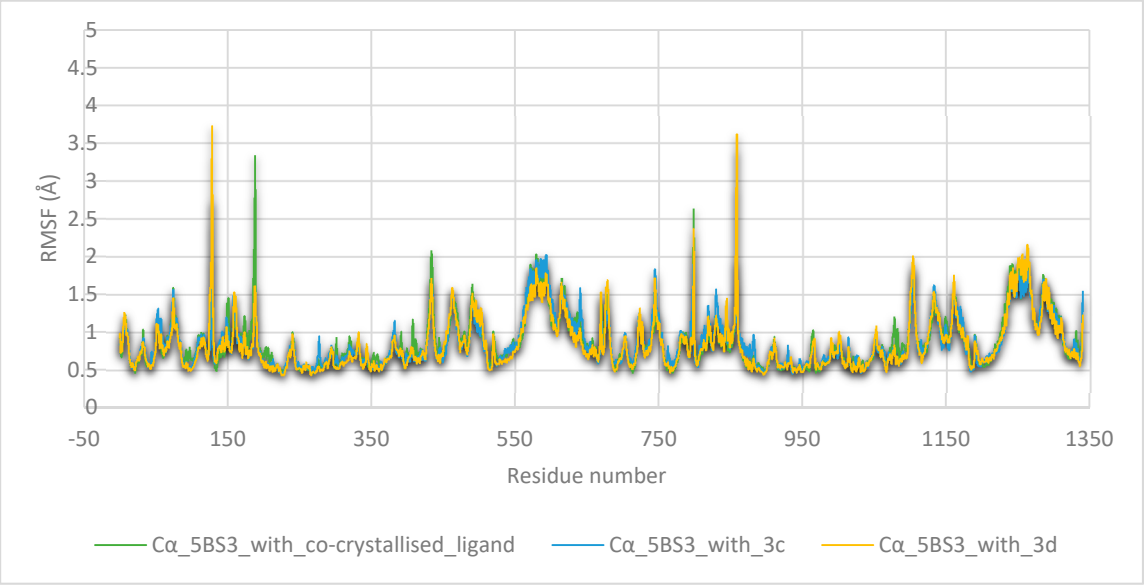

Figure S18. RMSF plot of the Cα atoms of *S. aureus* GyrA with co-crystallised tricyclic-1,5-naphthyridinone (compound 7) and compounds 3c and 3d at the NBTI site.

MM-GBSA binding free energies of ligand-receptor complexes during MD (Figures S19-S22)

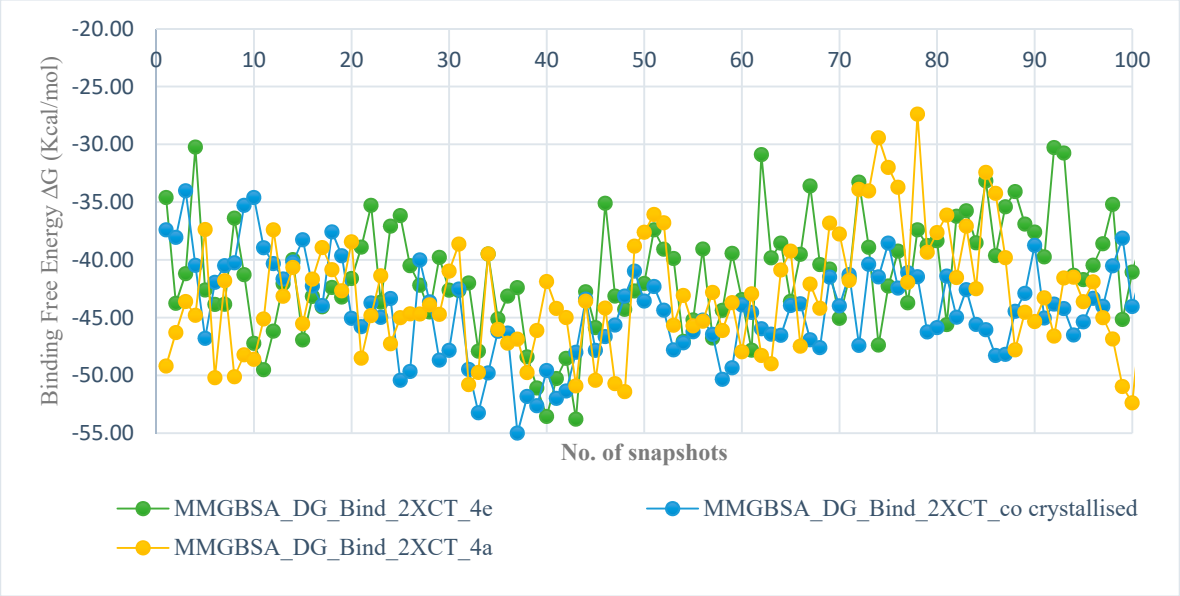

Figure S19. Prime/MM-GBSA binding free energy estimation for the ciprofloxacin and compound 4e at the fluoroquinolone binding site of *S. aureus* DNA gyrase subunit A (PDB ID: 2XCT) during a 10-ns MD simulation (snapshot structures of the complexes were evaluated at every 100 ps).

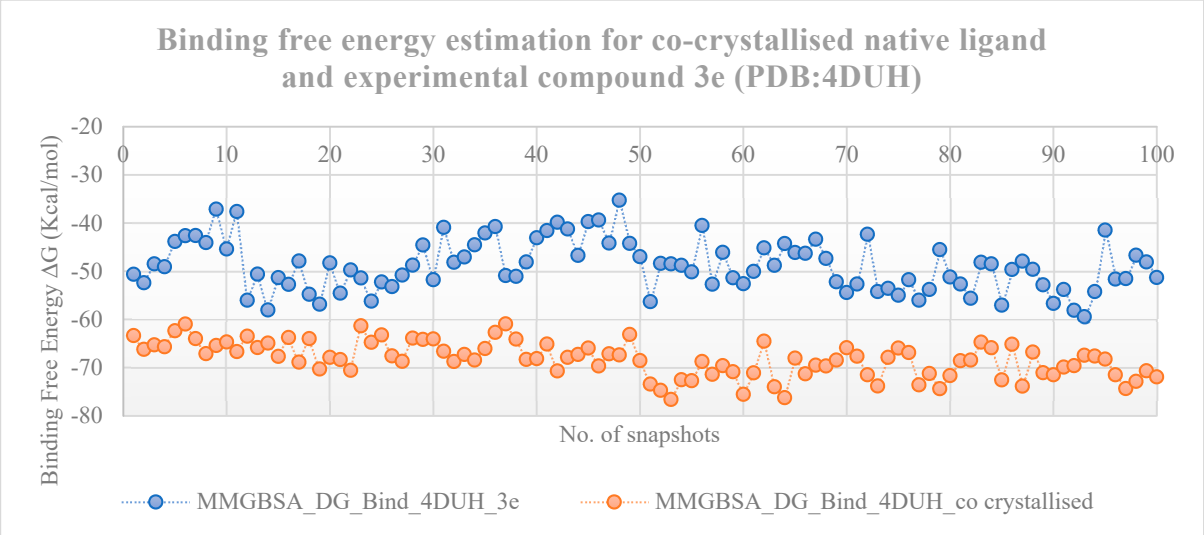

Figure S20. Prime/MM-GBSA binding free energy estimation for the co-crystallised 4,5'-bithiazole (inhibitor 18) and compound 3e at the coumarin binding site of *E. coli* DNA gyrase monomeric B subunit (PDB ID: 4DUH) during a 10-ns MD simulation (snapshot structures of the complexes were evaluated at every 100 ps).

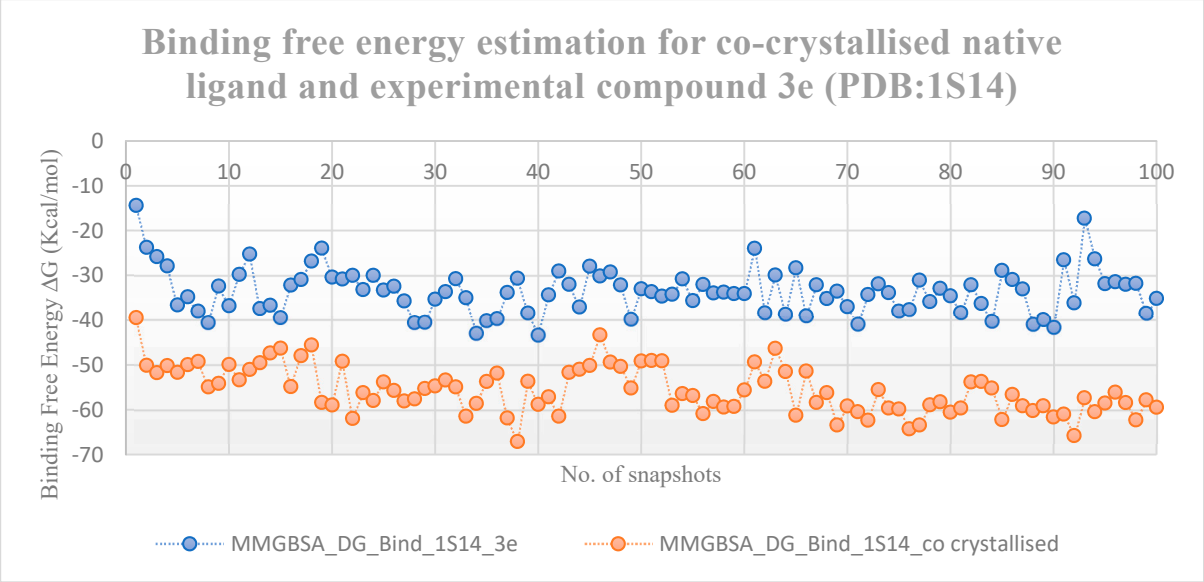

Figure S21. Prime/MM-GBSA binding free energy estimation for the co-crystallised novobiocin and compound 3e at the coumarin binding site of topoisomerase IV ParE subunit (PDB ID: 1S14) during a 10-ns MD simulation (snapshot structures of the complexes were evaluated at every 100 ps).

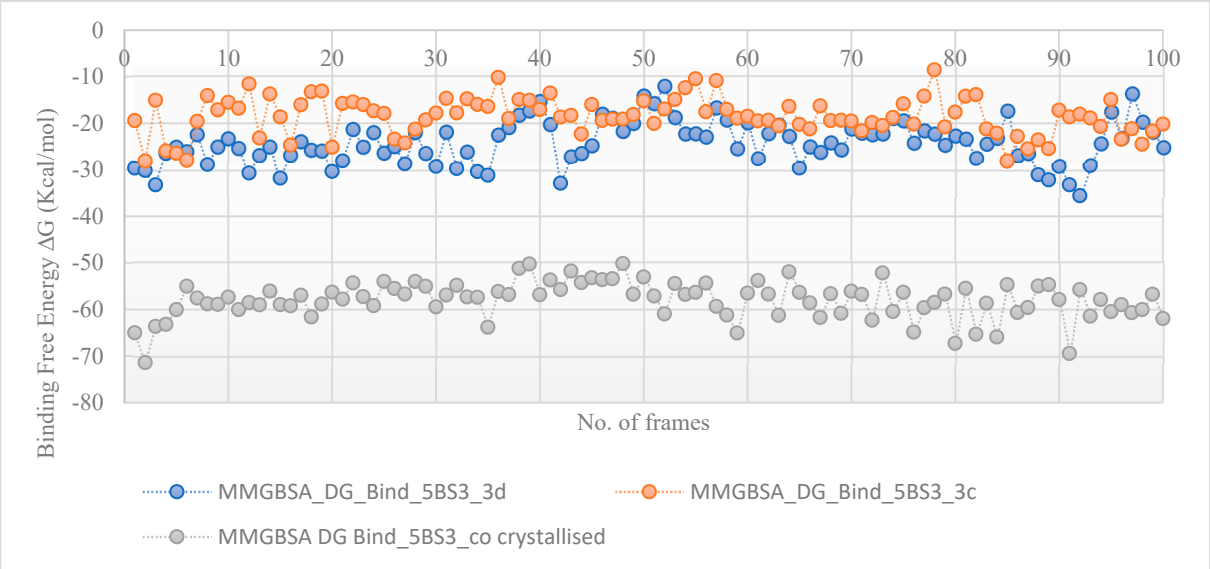

Figure S22. Prime/MM-GBSA binding free energy estimation for the co-crystallised crystallised tricyclic-1,5-naphthyridinone (compound 7) and compounds 3c and 3d at the NBTI binding site of *S. aureus* GyrA (PDB ID: 5BS3) during a 10-ns MD simulation (snapshot structures of the complexes were evaluated at every 100 ps).

Equilibration protocol before the MD production simulations

(i) 100 ps of Brownian dynamics at 10 K in the NVT ensemble, restraining the heavy atoms of the protein with a 50.0 kcal $mol^{-1}Å^{-1}$ force constant

(ii) 12 ps of Langevin dynamics at 10 K in the NVT ensemble using the Berendsen thermostat[10] with a relaxation time of 0.1 ps and short time steps (1-fs time step for bonded and near and 3-fs step for far) whilst restraining heavy atoms of the protein

(iii-iv) 12 ps of Langevin dynamics first at 10 K and then at 300 K and 1 atm pressure in the NPT ensemble using the Berendsen thermostat and barostat (relaxation times of 0.1 ps and 50.0 ps, respectively) with the same restraints

(v) 24 ps Langevin dynamics at 300 K in the NPT ensemble using the Berendsen thermostat and barostat (relaxation at 0.1 ps and 2 ps, respectively) without restrains.

NMR Spectra

Compound 3a

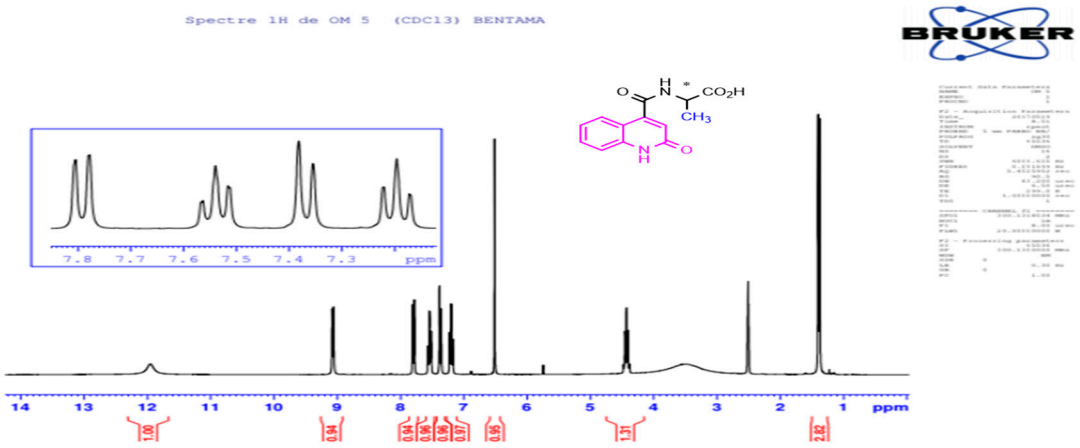

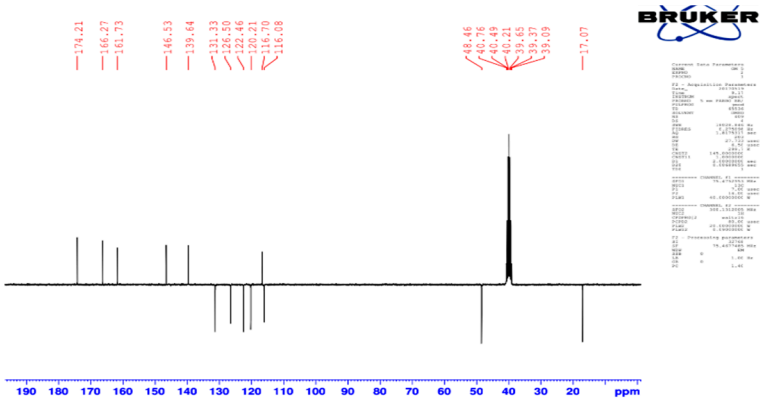

Compound 3b

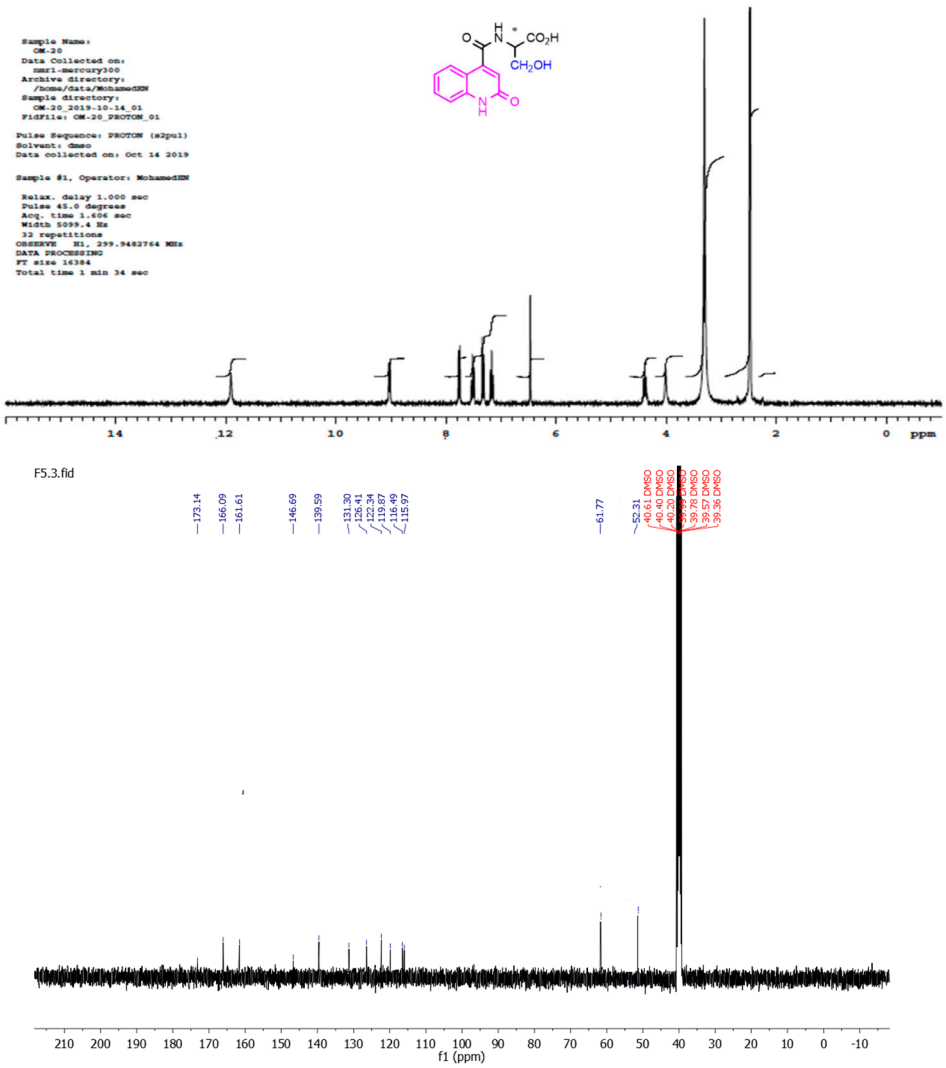
Sample Name:
OM-20
Data Collected on:
nmr1-mercury300
Archive directory:
/home/data/MohamedKN
Sample directory:
OM-20_2019-10-14_01
FidFile: OM-20_PROTON_01
Pulse Sequence: PROTON (s2pul)
Solvent: dmso
Data collected on: Oct 14 2019
Sample #1, Operator: MohamedKN
Relax. delay 1.000 sec
Pulse 45.0 degrees
Acq. time 1.606 sec
Width 5099.4 Hz
32 repetitions
OBSERVE H1, 299.9482764 MHz
DATA PROCESSING
FT size 16384
Total time 1 min 34 sec
CO2H
CH2OH
14
12
10
8
6
4
2
0
ppm
F5.3.fid
173.14
166.09
161.61
146.69
139.59
131.30
126.41
122.34
119.87
116.49
115.97
61.77
52.31
40.61 DMSO
40.40 DMSO
40.20 DMSO
39.99 DMSO
39.78 DMSO
39.57 DMSO
39.36 DMSO
210
200
190
180
170
160
150
140
130
120
110
100
90
80
70
60
50
40
30
20
10
0
-10
f1 (ppm)

Compound 3c

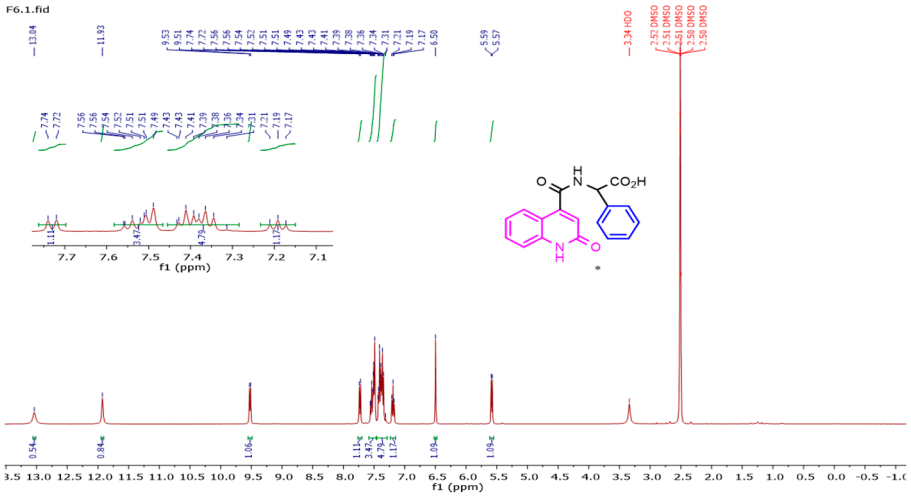

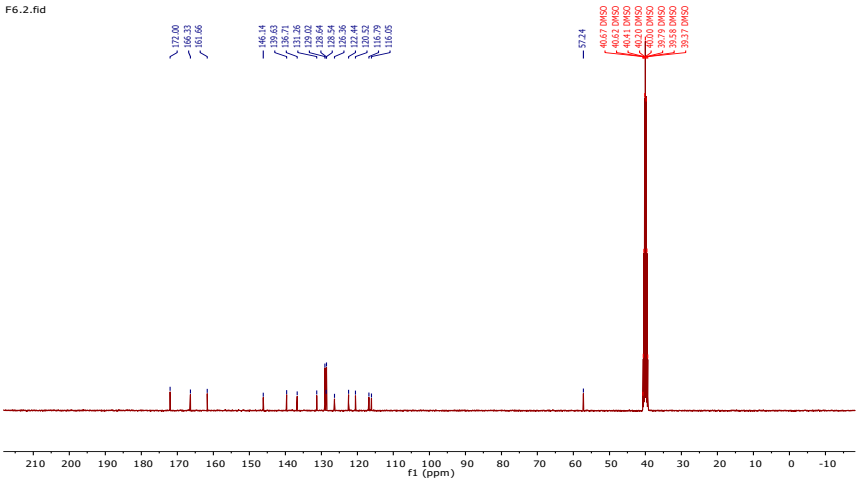

Compound 3d

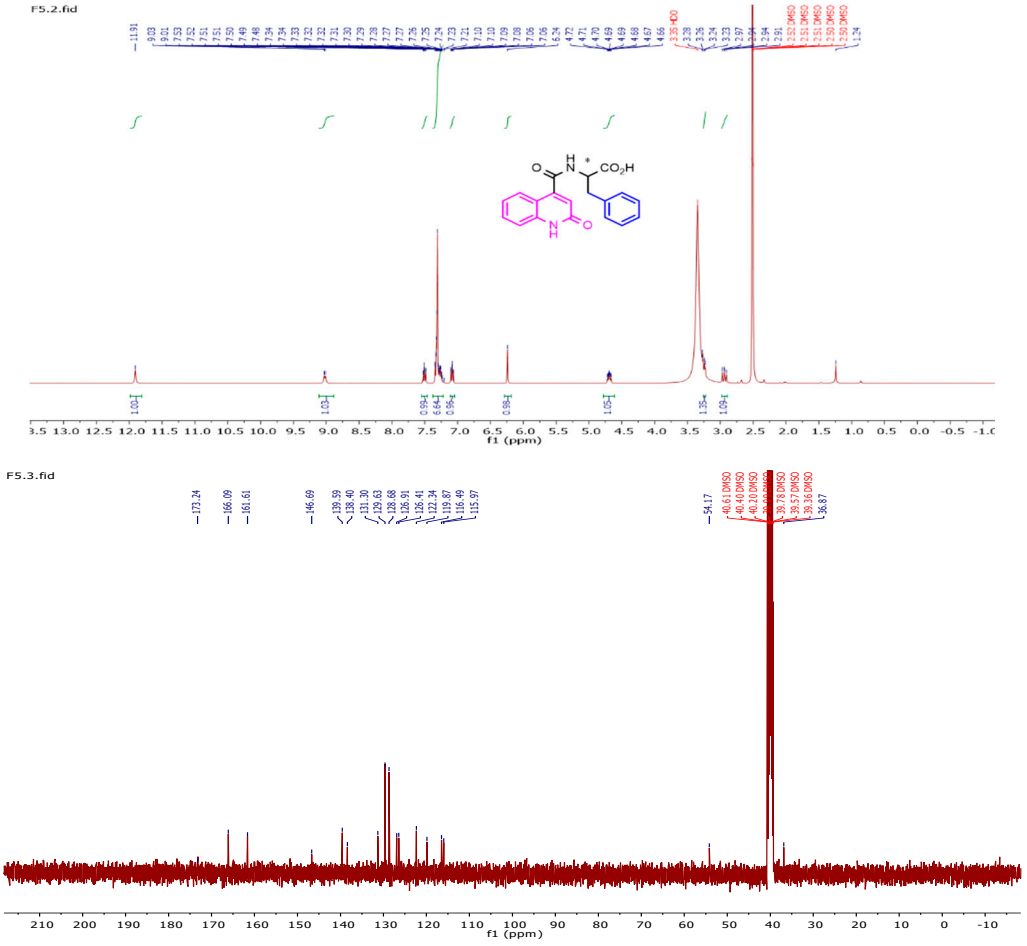

Compound 3e

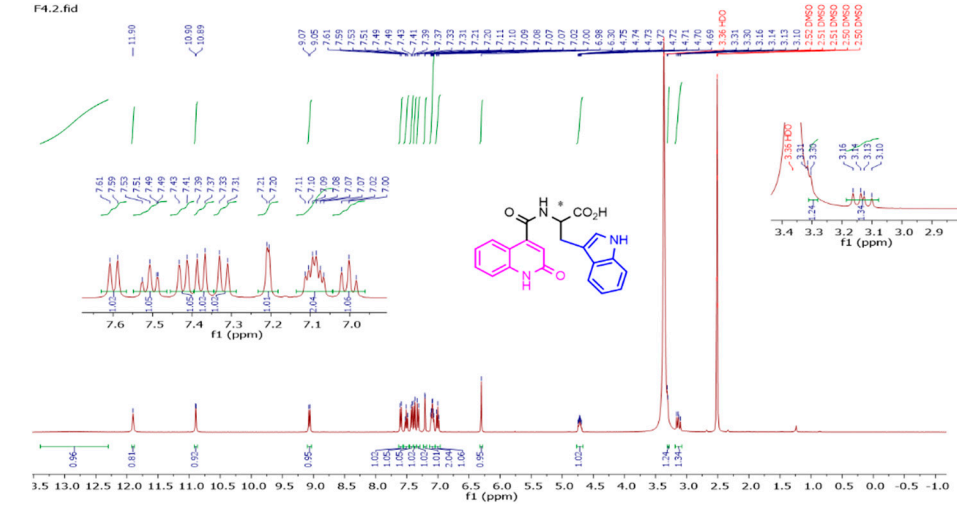

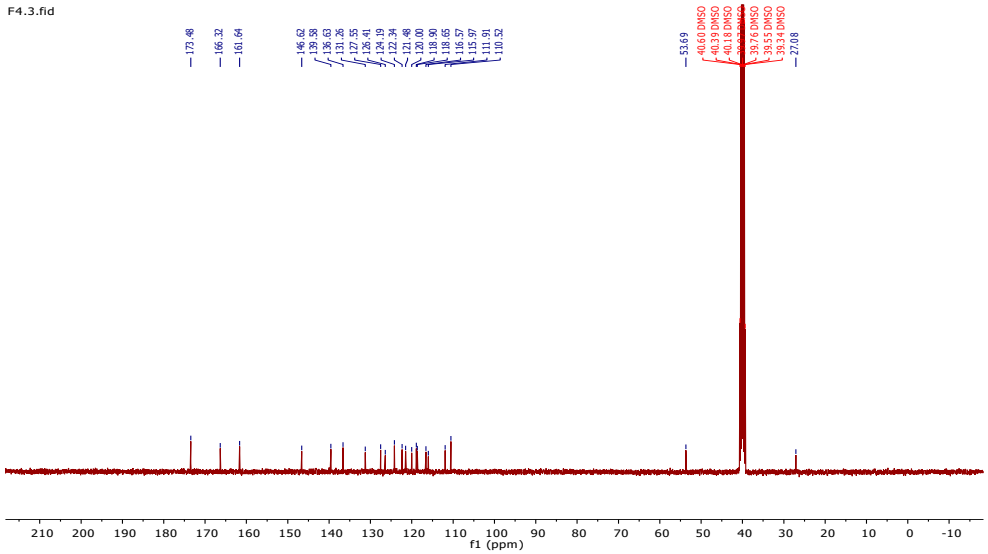

Compound 4a

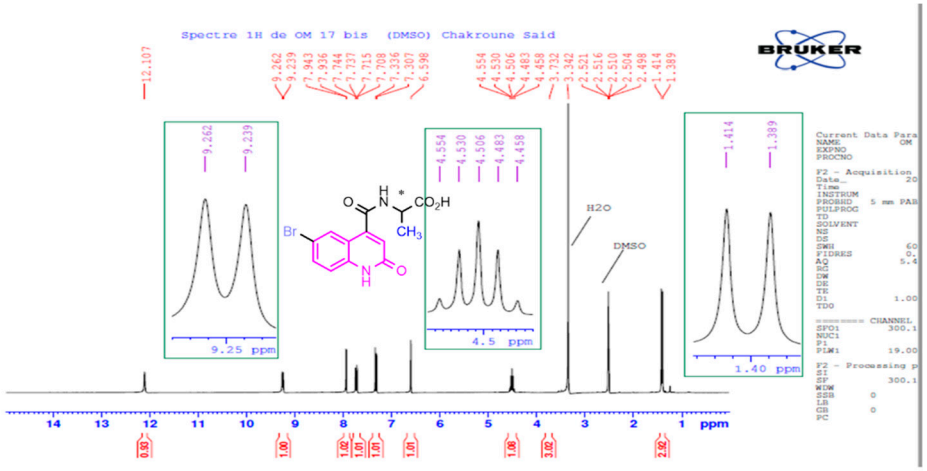
Spectre 1H de OM 17 bis (DMSO) Chakroune Said
BRUKER
H2O
DMSO
9.25 ppm
4.5 ppm
1.40 ppm
ppm

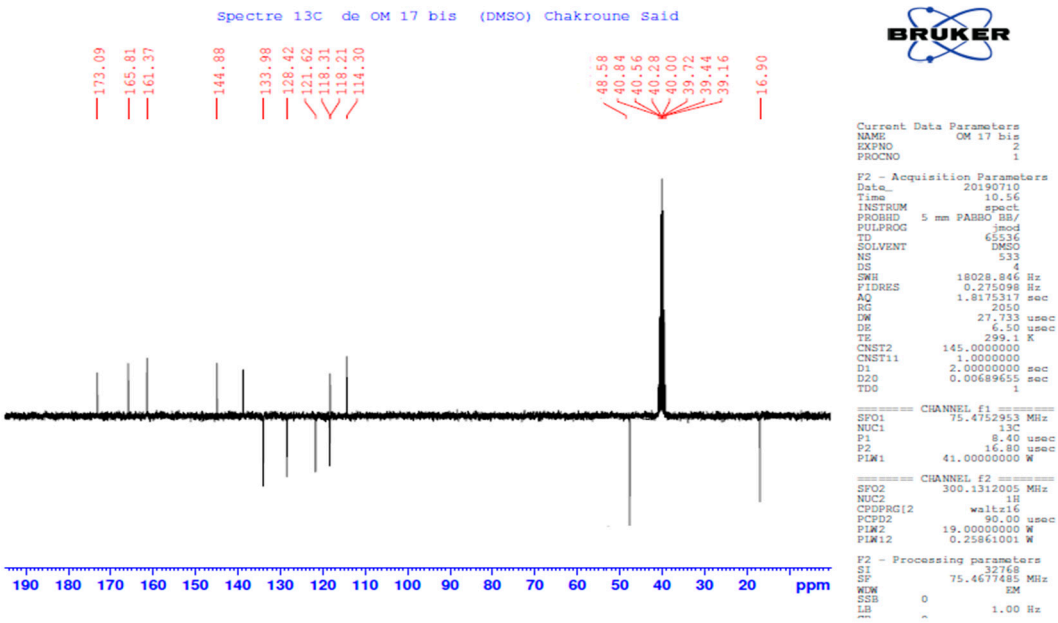
Spectre 13C de OM 17 bis (DMSO) Chakroune Said
BRUKER
ppm

Compound 4b

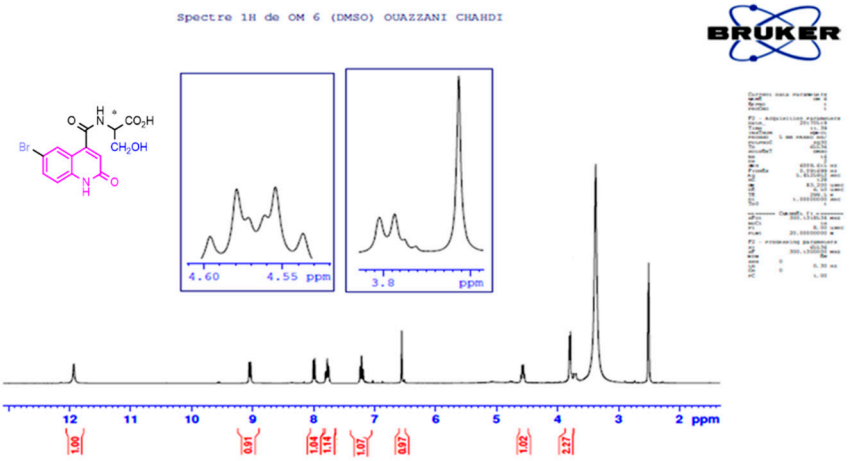
Spectre 1H de OM 6 (DMSO) OUAZZANI CHAHDI
BRUKER
4.60
4.55 ppm
3.8
ppm
12
11
10
9
8
7
6
5
4
3
2 ppm

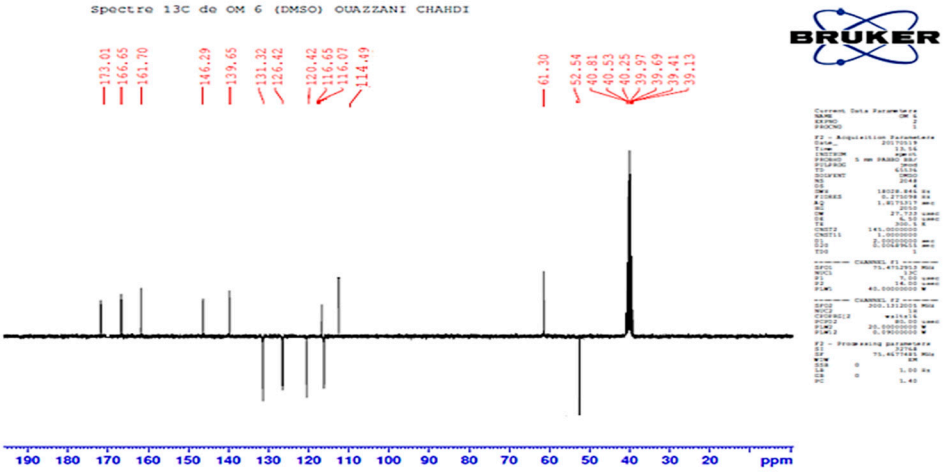
Spectre 13C de OM 6 (DMSO) OUAZZANI CHAHDI
BRUKER
173.01
166.65
161.70
146.29
139.65
131.32
126.42
120.42
116.65
116.07
114.49
61.30
52.54
40.81
40.53
40.25
39.97
39.69
39.41
39.13
190
180
170
160
150
140
130
120
110
100
90
80
70
60
50
40
30
20
ppm

Compound 4c

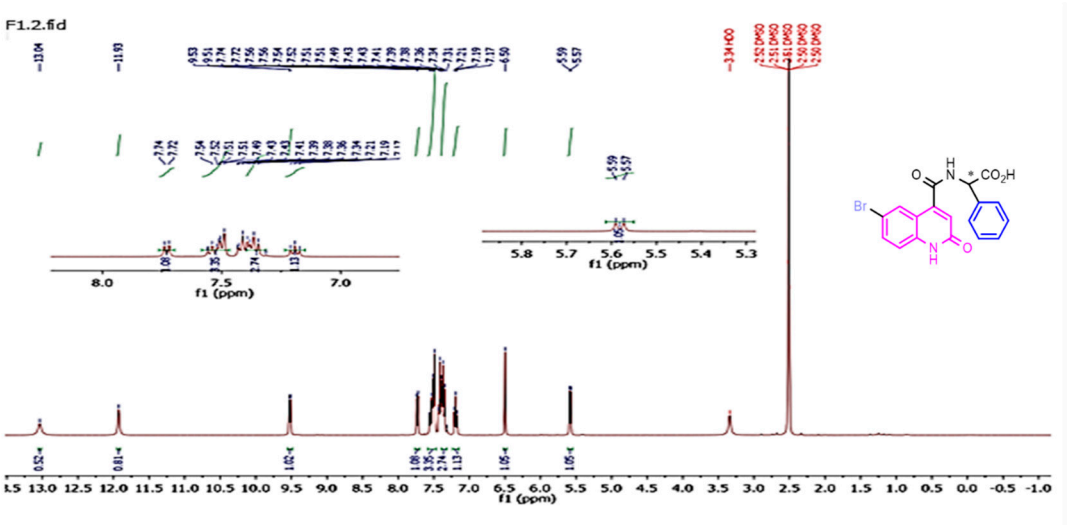

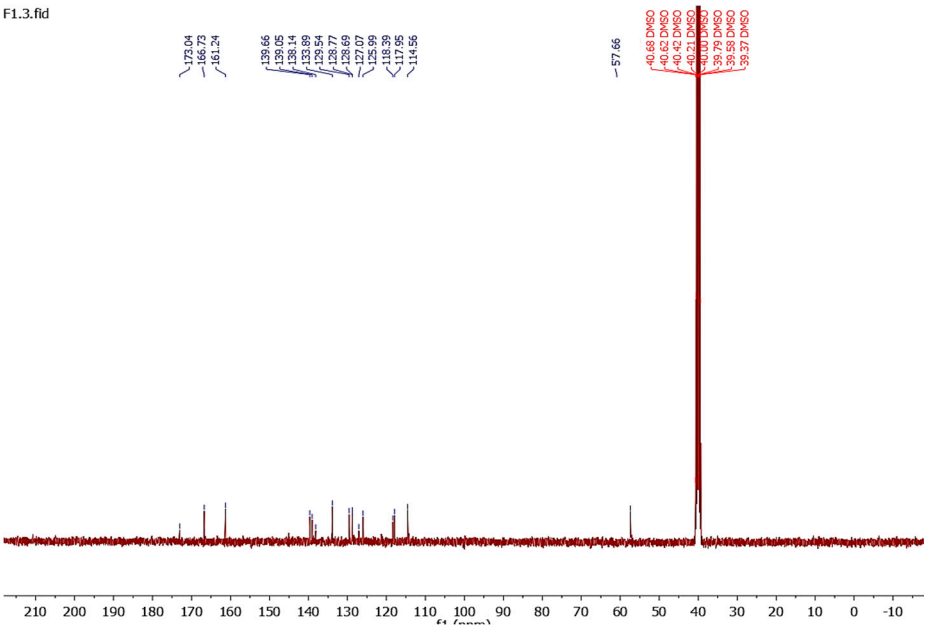

Compound 4d

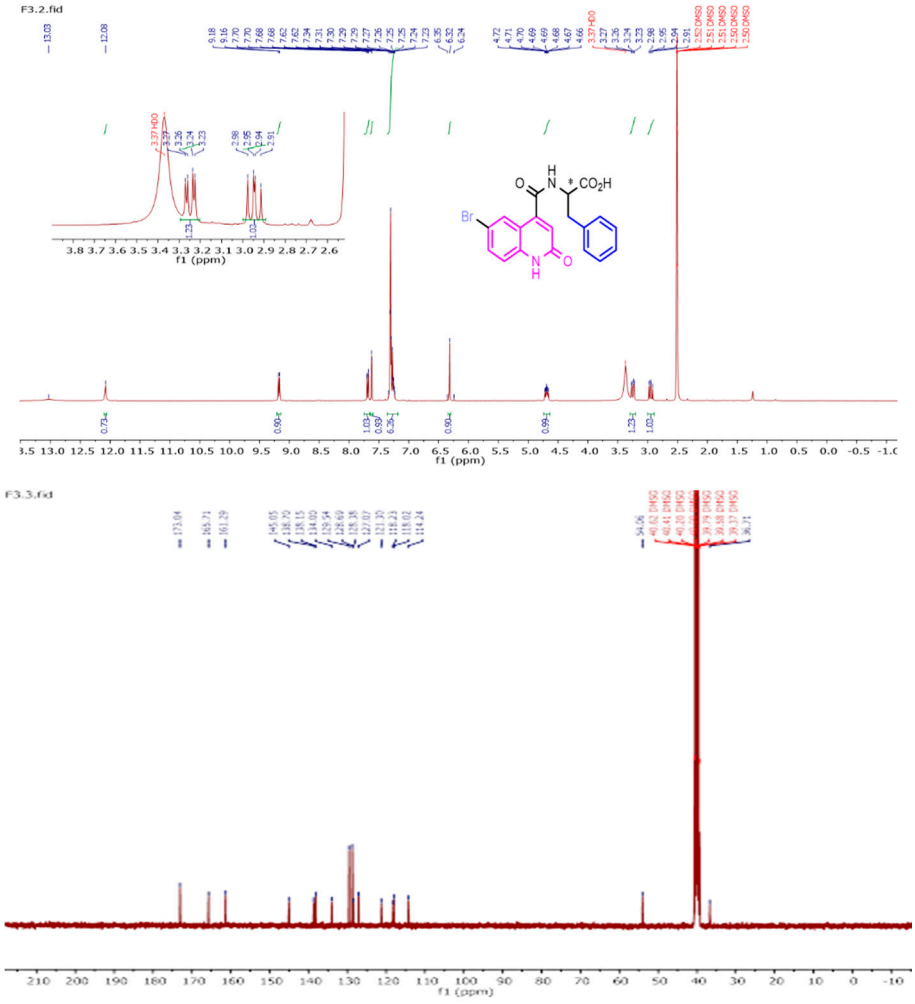

Compound 4e

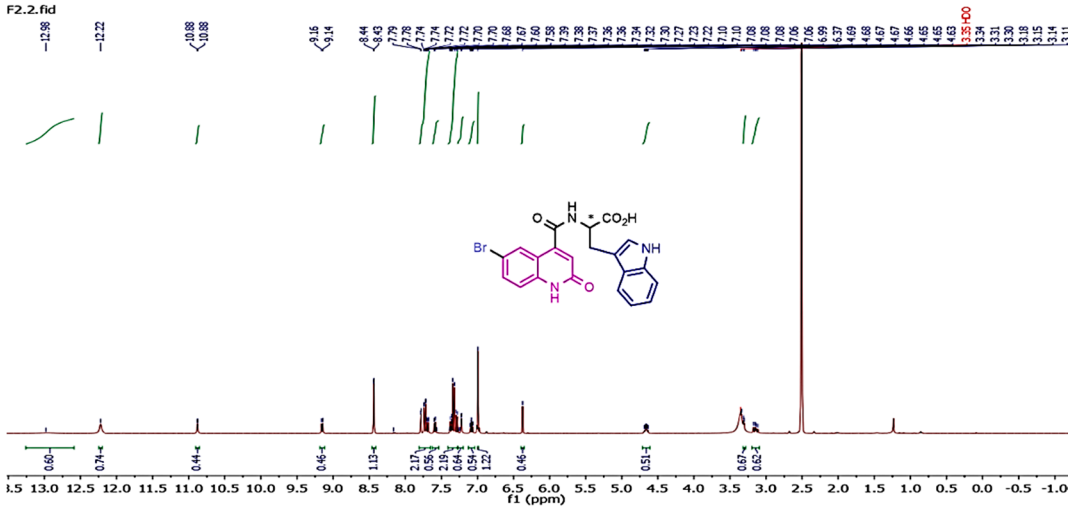
F2.2.fid
f1 (ppm)

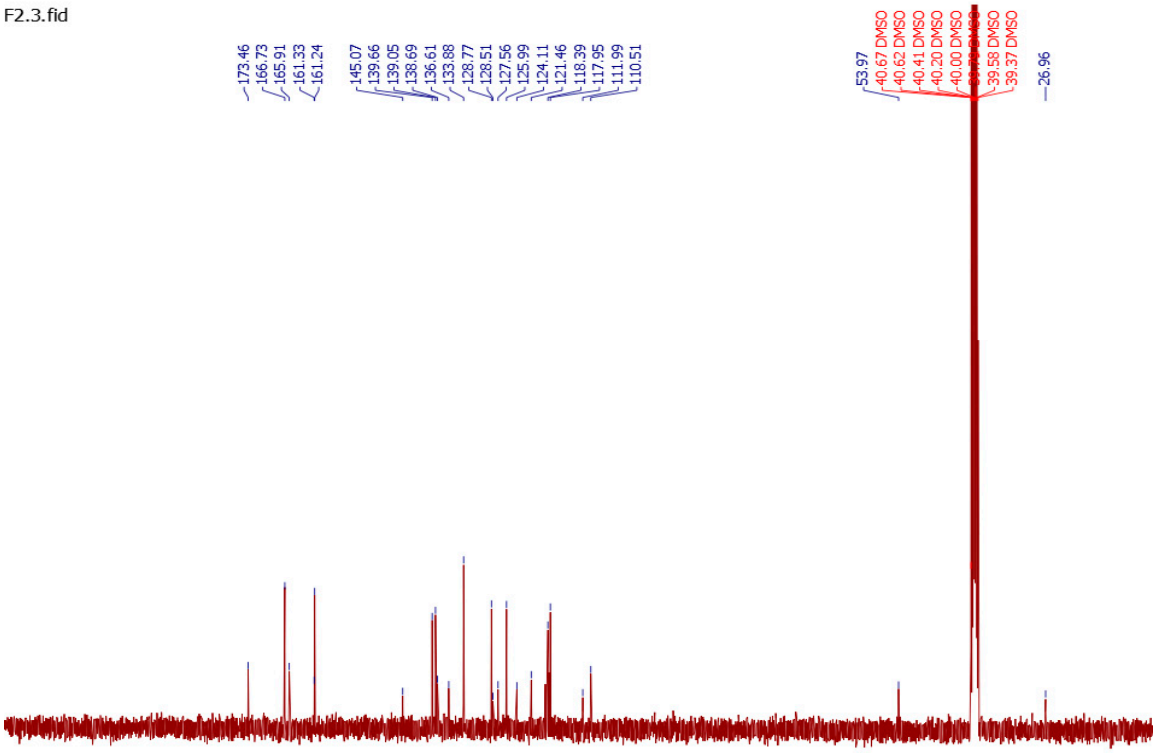
F2.3.fid
173.46
166.73
165.91
161.33
161.24
145.07
139.66
139.05
138.69
136.61
133.88
128.77
128.51
127.56
125.99
124.11
121.46
118.39
117.95
111.99
110.51
53.97
40.67 DMSO
40.62 DMSO
40.41 DMSO
40.20 DMSO
40.00 DMSO
39.58 DMSO
39.37 DMSO
26.96

References

(1) Edwards, M. J.; Flatman, R. H.; Mitchenall, L. A.; Stevenson, C. E. M.; Le Tung, B. K.; Clarke, T. A.; Mckay, A. R.; Fiedler, H. P.; Buttner, M. J.; Lawson, D. M.; Maxwell, A. *A Crystal Structure of the Bifunctional Antibiotic Simocyclinone D8, Bound to DNA Gyrase*; American Association for the Advancement of Science, 2009; Vol. 326, pp 1415–1418.

(2) Singh, S. B.; Kaelin, D. E.; Wu, J.; Miesel, L.; Tan, C. M.; Black, T.; Nargund, R.; Meinke, P. T.; Olsen, D. B.; Lagrutta, A.; Lu, J.; Patel, S.; Rickert, K. W.; Smith, R. F.; Soisson, S.; Sherer, E.; Joyce, L. A.; Wei, C.; Peng, X.; Wang, X.; Fukuda, H.; Kishii, R.; Takei, M.; Takano, H.; Shibasaki, M.; Yajima, M.; Nishimura, A.; Shibata, T.; Fukuda, Y. Tricyclic 1,5-Naphthyridinone Oxabicyclooctane-Linked Novel Bacterial Topoisomerase Inhibitors as Broad-Spectrum Antibacterial Agents-SAR of Left-Hand-Side Moiety (Part-2). *Bioorg. Med. Chem. Lett.* **2015**, *25*, 1831–1835. https://doi.org/10.1016/j.bmcl.2015.03.044.

(3) Singh, S. B.; Kaelin, D. E.; Wu, J.; Miesel, L.; Tan, C. M.; Meinke, P. T.; Olsen, D.; Lagrutta, A.; Bradley, P.; Lu, J.; Patel, S.; Rickert, K. W.; Smith, R. F.; Soisson, S.; Wei, C.; Fukuda, H.; Kishii, R.; Takei, M.; Fukuda, Y. Oxabicyclooctane-Linked Novel Bacterial Topoisomerase Inhibitors as Broad Spectrum Antibacterial Agents. *ACS Med. Chem. Lett* **2014**, *5*, 12. https://doi.org/10.1021/ml500069w.

(4) Gibson, E. G.; Bax, B.; Chan, P. F.; Osheroff, N. Mechanistic and Structural Basis for the Actions of the Antibacterial Gepotidacin against Staphylococcus Aureus Gyrase. *ACS Infect. Dis.* **2019**, *5* (4), 570–581. https://doi.org/10.1021/acsinfecdis.8b00315.

(5) Stanger, F. V.; Dehio, C.; Schirmer, T. Structure of the N-Terminal Gyrase B Fragment in Complex with ADP·Pi Reveals Rigid-Body Motion Induced by ATP Hydrolysis. *PLoS One* **2014**, *9* (9), e107289. https://doi.org/10.1371/journal.pone.0107289.

(6) Geoffrey A. Holdgate; Alan Tunnicliffe, §; Walter H. J. Ward; Simon A. Weston; Gina Rosenbrock; Peter T. Barth; Ian W. F. Taylor; Richard A. Pauptit, and; Timms*, D. The Entropic Penalty of Ordered Water Accounts for Weaker Binding of the Antibiotic Novobiocin to a Resistant Mutant of DNA Gyrase: A Thermodynamic and Crystallographic Study‡. **1997**. https://doi.org/10.1021/BI970294+.

(7) Vanden Broeck, A.; McEwen, A. G.; Chebaro, Y.; Potier, N.; Lamour, V. Structural Basis for DNA Gyrase Interaction with Coumermycin A1. *J. Med. Chem.* **2019**, *62* (8), 4225–4231. https://doi.org/10.1021/acs.jmedchem.8b01928.

(8) Mesleh, M. F.; Cross, J. B.; Zhang, J.; Kahmann, J.; Andersen, O. A.; Barker, J.; Cheng, R. K.; Felicetti, B.; Wood, M.; Hadfield, A. T.; Scheich, C.; Moy, T. I.; Yang, Q.; Shotwell, J.; Nguyen, K.; Lippa, B.; Dolle, R.; Ryan, M. D. Fragment-Based Discovery of DNA Gyrase Inhibitors Targeting the ATPase Subunit of GyrB. *Bioorganic Med. Chem. Lett.* **2016**, *26* (4), 1314–1318. https://doi.org/10.1016/j.bmcl.2016.01.009.

(9) Sherer, B. A.; Hull, K.; Green, O.; Basarab, G.; Hauck, S.; Hill, P.; Loch, J. T.; Mullen, G.; Bist, S.; Bryant, J.; Boriack-Sjodin, A.; Read, J.; Degrace, N.; Uria-Nickelsen, M.; Illingworth, R. N.; Eakin, A. E. Pyrrolamide DNA Gyrase Inhibitors: Optimization of Antibacterial Activity and Efficacy. *Bioorganic Med. Chem. Lett.* **2011**, *21* (24), 7416–7420. https://doi.org/10.1016/j.bmcl.2011.10.010.

(10) Berendsen, H. J. C.; Postma, J. P. M.; Van Gunsteren, W. F.; Dinola, A.; Haak, J. R. Molecular Dynamics with Coupling to an External Bath. *J. Chem. Phys.* **1984**, *81* (8), 3684–3690. https://doi.org/10.1063/1.448118.